THE DYNAMICS OF BI-DIRECTIONAL EXCHANGE FLOWS: IMPLICATIONS FOR MORPHODYNAMIC CHANGE WITHIN ESTUARIES

Claudia Adduce (1), Maria Chiara De Falco (1), Alan Cuthbertson (2), Janek Laanearu (3), Daniela Malcangio (4), Katrin Kaur (3), Eletta Negretti (5), Joel Sommeria (5), Thomas Valrha (5) & Samuel Viboud (5)

(1) University Roma Tre, Italy, E-mail: claudia.adduce@uniroma3.it
(2) University of Dundee, School of Science and Engineering, UK, E-mail: a.j.s.cuthbertson@dundee.ac.uk
(3) Tallinn University of Technology, Estonia, E-mail: janek.laanearu@taltech.ee
(4) Polytechnic University of Bari, Italy, E-mail: daniela.malcangio@poliba.it
(5) Laboratory of Geophysical and Industrial Flows, France, E-mail: joel.sommeria@univ-grenoble-alpes.fr

An experimental study has been conducted at the CNRS Coriolis Rotating Platform at LEGI, Grenoble, in a trapezoidal cross section channel, to investigate uni and bi-directional exchange flows. Both rotating and non rotating experiments, with a non-erodible and erodible bed layer were considered. Experimental measurements focused on obtaining high-resolution velocity and density fields in different vertical planes spanning the width of the channel using 2D Particle Image Velocimetry, Laser Induced Fluorescence, ADV and micro-conductivity probes in several channel sections. Preliminary results from the study are presented herein and consider the exchange flow dynamics at the interface, with particular focus on the observed cross-channel variations in the counter-flowing water masses and layer thickness. Further analyses are ongoing to improve understanding of the interfacial mixing and entrainment/detrainment processes, along with the bed-morphological changes initiated by interaction mechanisms between the erodible bottom boundary and the uni- or bi-directional exchange flows.

1. INTRODUCTION

Uni-directional gravity currents and bi-directional exchange flows occur within estuaries, tidal inlets and sea straits when horizontal density differences (i.e. baroclinic forcing) and/or pressure gradients (i.e. barotropic forcing) are present between the adjacent water bodies. The nature of these buoyancy-driven flows depends on whether Coriolis effects due to the Earth's rotation play a significant role in the internal flow dynamics (depending on the scale of the environmental/geophysical flow under consideration), as well as the strong topographic controls imposed by seafloor bathymetry and channel shape. These factors are known to exert significant influence on both internal mixing and secondary circulations generated by exchange flows (e.g. Kõuts and Omstedt, 1993; Johnson and Ohlson, 1994; Andrejev et al., 2004; Laanearu et al., 2014). In such cases, the flow dynamics of the dense lower layer depend primarily on the volumetric flux and channel cross-sectional shape, while the stratified interfacial flow mixing characteristics, leading to fluid entrainment/detrainment, are also dependent on the buoyancy flux and motion within the upper (lower density) water mass (i.e. bi-directional exchange flow). Furthermore, when submerged channels are relatively wide in comparison to the internal Rossby radius of deformation, Earth rotation effects introduce geostrophic adjustment of these internal fluid motions (e.g. Cuthbertson et al, 2011) that can suppress turbulent mixing generated at the interface (e.g. Maxworthy, 1985) and result in the development of Ekman layers that induce secondary, cross-channel circulations (e.g. Johnson and Ohlson, 1994; Cossu et al., 2010), even within straight, rectangular channels.

Understanding of these uni- and bi-directional flow processes is particularly relevant in coastal regions, where water and nutrient exchanges between both tidal and non-tidal inlets (e.g. estuaries, lagoons) and open marine waters are strongly regulated by channel topography and bathymetric features (Cuthbertson et al., 2006). This has significant implications for the intrusion of saline marine waters and flushing of semi-enclosed estuarine impoundments, fjords and regional seas (Matthäus and Lass, 1995; Farmer and Armi, 1999). Furthermore, as many tidal inlets and estuaries

exhibit complex morphological patterns consisting of channels and shoals with strong spatial and temporal variability (e.g. Schramkowski and de Smart, 2002), it is important to understand how the evolution of these topographical features produces an associated feedback on internal flow dynamics. Specifically, the interaction between channel bathymetry and exchange flows under the influence of boundary friction and earth rotation has been shown analytically (Valle-Levinson et al., 2003) to result in transverse asymmetries in the structure of the along-estuary flows, which disappear under strongly frictional (i.e. high Ekman number) conditions. In addition, the cross-channel structure of secondary flows, controlled by the balance between pressure gradient and friction, can reverse in direction under very weak friction, reflecting Coriolis deflection of along-estuary flows (i.e. geostrophic adjustment). It is therefore expected that, for both uni-directional currents and bi-directional exchange flows generated over deformable channels (e.g. estuaries), the physical interactions between the lower dense water flow and the erodible bed will have a strong influence in reshaping channel morphology (e.g. Schramkowski and de Swart, 2002). This changing morphology is thus expected to have associated feedback on transverse asymmetries associated with uni-directional currents and bi-directional exchange flows (e.g. velocity distributions; maximum velocity thalweg; secondary flow circulations), as well as on their internal flow stability (e.g. stratification; interfacial mixing; entrainment) (e.g. Valle-Levinson et al., 2003).
In the current study, the behaviour of uni-directional gravity currents and bi-directional exchange flows along a trapezoidal-shaped channel with a rigid and erodible bottom topography is investigated to determine the relative influence of the channel geometry and Coriolis forces on the lateral distribution of the (counter-)flowing water masses, interfacial mixing and secondary flow generation, as well as the feedback from bed deformation on these internal flow processes. Recent studies (e.g. Cuthbertson et al, 2011; 2014; Laanearu et al, 2014) of uni-directional, dense gravity currents generated in rotating and non-rotating systems indicated that a rigid, V-shaped channel topography had a strong influence on both flow distribution and associated interfacial mixing characteristics along the channel. Similar topographic controls on bi-directional exchange flows in rotating and non-rotating systems, along with their impact on (and feedback from) deformable channel bed conditions have not yet been fully resolved.

The current paper reports initial findings from a parametric experimental study conducted at the Coriolis Rotating Platform at LEGI Grenoble in Spring/Summer 2018, which was aimed at filling existing knowledge gaps associated with enhanced understanding of (i) the physical nature of exchange flow-bathymetry feedback within deformable channels; (ii) interfacial mixing, secondary flow circulations and near-bed boundary dynamics; and (iii) the external parametric influences of tidal/freshwater forcing, density differences, bed friction and Coriolis effects on these exchange flow-topography interactions

2. EXPERIMENTAL APPARATUS

Laboratory experiments were conducted in the CNRS Coriolis Rotating Platform at Laboratoire des Ecoulements Geophisiques et Industriels (LEGI) in Grenoble, which consists of a 13 m diameter and 1.2 m deep circular tank that can be rotated at a constant angular velocity. For the current experimental configuration, a trapezoidal cross-section channel of length 6.5 m (Figure 1) was positioned in the tank. This channel was constructed from transparent Plexiglas to facilitate flow visualization along its length.

Entry and exit slopes ($\alpha_b = 26.57°$) connected the main channel section to the inlet basin (B) and outlet basin (A). The trapezoidal section had a 2 m top width, 1 m bottom width and 0.5 m total depth, with side slopes of $\alpha_s = 45°$. A 0.1 m deep sediment trap, running the full length of the channel, was built into the trapezoidal channel arrangement to perform the experiments with an erodible bed layer, while a rigid Plexiglas bottom was used for the non-erodible bed experiments. The sediments used were polystyrene particles with representative nominal diameter $D_n = 310\ \mu m$, density $\rho_s = 1040\ kg/m^3$ and settling velocity of the particles $v_s = 0.15\ cm/s$ based on Stokes law for an isolated spherical grain. Before commencing the erodible bed experiments, the sediment bed layer contained within the trap was leveled manually in order to provide the same initial boundary condition as for the equivalent non-erodible bed experiments. At the beginning of each experiment the circular tank was filled with freshwater at density ρ_2, to a total depth $H = 0.9\ m$, with a corresponding submergence depth in the channel $h = 0.4\ m$. For the rotating experiments, the platform was spun-up slowly to reach a fixed angular velocity and attain a state of rigid body rotation after several hours.

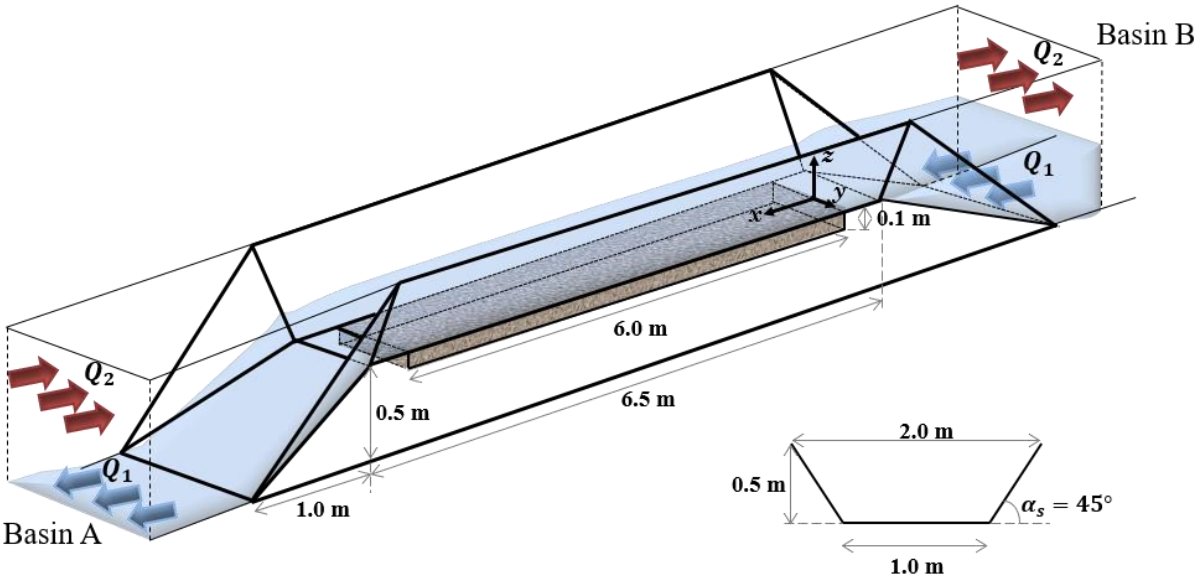

Figure 1 Schematic representation of the experimental apparatus in the LEGI Coriolis Platform

The saline water at density ρ_1 was delivered through a gravity feed system to the bottom of Basin B, via a rectangular manifold, filling up basin B slowly (to minimize mixing) until the dense water interface reached the elevation of the channel bottom. At this point, a prescribed, constant saline water discharge Q_1 was fed into basin B to establish a stable, uni-directional flow along the trapezoidal channel. The same flow rate was extracted from outside of the channel (through the drainage system in the circular tank) to ensure the water depth in the channel remained constant. Two water pumps in the upper part of Basin B provided a constant fresh water flux Q_2 within the channel to generate a bi-directional exchange flow, once the saline water outflow was fully established.

Experimental measurements were targeted at obtaining high temporal and spatial resolution density and velocity fields across the channel, particularly within a central 1 m-long section of the 6.5 m long trapezoidal channel (i.e. away from the converging and upsloping approaches from basins A and B). This central section was selected to ensure that the exchange flow conditions generated through the channel at this location could be assumed to be fully geostrophically-adjusted. To this aim, two-dimensional Particle Image Velocimetry (PIV) and Laser Induced Fluorescence (LIF) were used to obtain measurements in vertical (XZ) planes along this central region of the trapezoidal channel (Figure 2a).

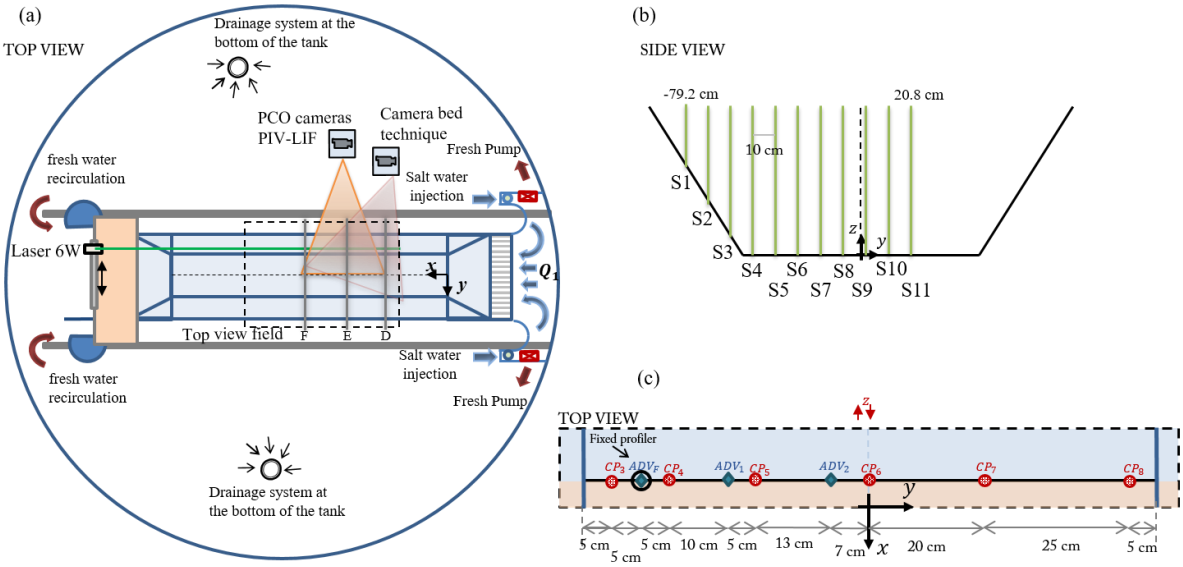

Figure 2 Schematic representation of (a) top view configuration of the channel and experimental set-up in the circular tank, (b) side view of the PIV planes and (c) top view of the ADV measurement locations.

A 6 W YAG laser, mounted on a traverse system on the side of the tank, provided a movable vertical laser sheet, aligned along the x-direction, spanning the channel width. This set-up allowed velocity and density fields to be obtained in 11 vertical sections (XZ) at lateral positions ranging between -79.2 cm < y < 20.8 cm (Figure 2b), at lateral intervals of 10 cm. These velocity (PIV) and density (LIF) fields were acquired by two PCO high-speed, digital cameras with a spatial resolution of 2560x2160 pixels and frame rate set at 10 Hz. For the LIF and flow visualization, Rhodamine 6G was added to the saline water at a constant concentration.

The PIV and LIF measurements were obtained by scanning the 11 vertical sections 3 times over a 30 second duration for each field. Moreover, rapid-deploying measurements were performed by profiling probes positioned on a transect arm across the trapezoidal channel and overlapping the central area of interest and PIV-LIF fields [at 3 locations, namely Section D, E and F (Figure 2a,c)]. In particular, 6 micro-conductivity probes distributed on the cross-section (Figure 2c) were used to measure the instantaneous density profiles, while one side-looking and one down-looking Acoustic Doppler Velocimeter (ADV) were positioned with their sampling volumes at an equivalent vertical elevation to the micro-conductivity probes tips to collect coupled velocity profiles. An additional ADV profiler was positioned at a fixed elevation to measure the near bed velocity field.

A bottom-boundary visualisation technique, using the vertical laser sheet, was implemented to measure deformations in the erodible bed. A digital camera (resolution 4096 x 3072 pixels) placed outside the trapezoidal channel was used to acquire at a frame rate of 20 Hz the bed-shape before and after each experiment, in the central region of the channel, 2.8 m long and 0.9 m thick. A geometrical calibration was applied and allowed to evaluate the bed surface elevations from the initial undisturbed conditions. Finally, an additional camera positioned on the top of the circular tank provided a global field of the experimental runs.

3. LABORATORY EXPERIMENTS

Four experimental configurations were considered in the project:

- Case 1: uni / bi-directional exchange flows in a non-rotating, rigid-bottom channel.
- Case 2: uni / bi-directional exchange flows in a rotating, rigid-bottom channel
- Case 3: uni / bi-directional exchange flows in a non-rotating channel with an erodible bed.
- Case 4: uni / bi-directional exchange flows in a rotating channel with an erodible bed.

Within all experiments, the flow rate of the salty water Q_2 was kept constant ($Q_2 = 4.4\ l/s$), while the flow rate of the fresh water Q_1 was increased over a range of values ($Q_1 = 0, 8, 20\ l/s$). The rotation of the Coriolis Platform was varied with four angular velocities Ω tested (i.e. $\Omega = 0, 0.05, 0.1, 0.2\ rad/s$). The density difference of fresh and saline water flows was maintained constant and equal to $\Delta\rho = 10\ kg/m^3$ for most of the experiments, with a limited number of experiments with the erodible bed layer performed at a higher density difference $\Delta\rho = 20\ kg/m^3$. The main parameters investigated in the experimental runs are thus (i) the relative magnitude of fresh and saline water volume fluxes $q^* = Q_1/Q_2$, (ii) the density difference $\Delta\rho$ and (iii) the angular velocity Ω of the rotating circular tank, both with a rigid bottom channel (Case 1-2) and an erodible bed layer (Case 3-4).

4. PRELIMINARY RESULTS

In this section an overview of the preliminary results of the experiments with the rigid-bottom condition is presented. In particular, the PIV measurements permit us to obtain detailed information on the spatial flow structure of the upper and lower layers. Figure 3 shows, for $\Omega = 0\ rad/s$, the time averaged velocity vector field, while the background color map details the absolute value of the horizontal time-averaged velocity component at PIV section S9 (i.e. $y = 0.8\ m$, approximately along the channel centerline). Here, the initial gravity current experiment (i.e. $q^* = 0$, Figure3a) and the subsequent bi-directional exchange flow condition ($q^* = 1.8$, Figure3b) are compared to highlight the effect of the upper fresh water volume flux Q_1. Indeed, for the same Ω, the increase of the upper layer flux Q_1 results in a reduction of the lower saline layer thickness h_c, defined by $u = 0\ cm/s$ interface, and a slight increase of the velocity of the lower saline flow u_2. Moreover, a

constant increase of the time averaged velocity u_1 in the upper layer flow is observed, as a consequence of the increasing upper fresh water flow Q_1.
In Figure 4, the effect of the rotation rate on the gravity current development along the trapezoidal channel is shown (i.e. $q^* = 0$). The non-rotating experiment (i.e. $\Omega = 0\, rad/s$, Figure 4a-b) and the rotating case with $\Omega = 0.05\, rad/s$ (Figure 4c-d) are compared in Sections S3 ($y = -59.2\, cm$) and S4 ($y = -49.2\, cm$) located on the side slope of the trapezoidal section and on the horizontal bottom of the channel, respectively.

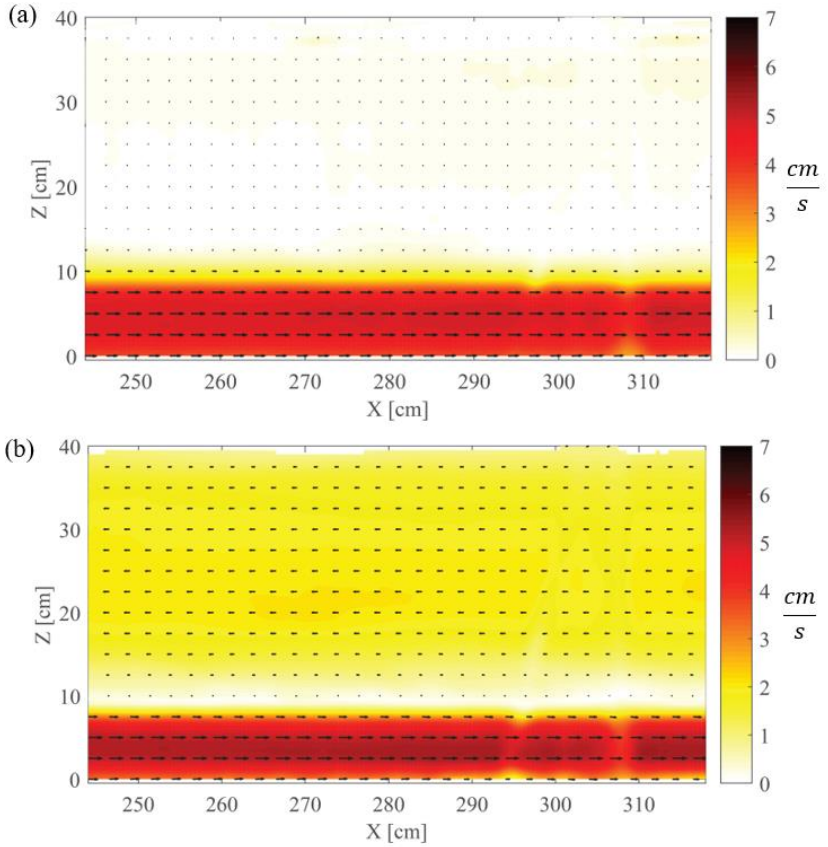

Figure 3 PIV velocity fields at section S9 and colormap of the absolute value of u for Ω=0 rad/s and (a) q=0, (b) q*=1.4.*

In Figures 4a & 4c, the time averaged velocity vector field and the color map of the magnitude of the horizontal time-averaged velocity component u, are shown at section S3 for the $\Omega = 0\, rad/s$ and $\Omega = 0.05\, rad/s$, respectively. These indicate the clear inclination of the cross-channel interface between the upper fresh and lower saline layers, induced by the non-zero angular velocity. Indeed, for the non-rotating case (Figure 4a), the absence of lower saline layer from the velocity field indicates that the saline layer has a thickness lower than the minimum z elevation of PIV section S3 on the sloping side wall ($z = 9.2\, cm$). By contrast, in the rotating case (Figure 4c), the elevation of the $u = 0\, cm/s$ interface lower saline and upper fresh water fluxes is observed at $h_c = 14\, cm$, indicating that the saline flow is directed to the right side of the channel (in the direction of the saline flow) due to the non-zero angular rotation of the channel. Furthermore, in PIV section S4 (Figures 4b & 4d), an increase in the thickness of the saline flow layer is observed, with a corresponding decrease in the lower layer velocity u_2.

The cross channel variation in the $u = 0\, cm/s$ interface elevation is shown in Figure 5 in the measured PIV sections for the three q^* values tested. The non-rotating experiments (Figure 5a) are compared with the experiments with an angular velocity $\Omega = 0.05\, rad/s$ (Figure 5b) to highlight the influence of the rotation on the internal fluid motions. In particular for $\Omega = 0\, rad/s$, the effect of the increasing upper fresh water flow (i.e. increasing q^*) is to reduce the lower layer thickness. Whereas, when the angular rotation Ω plays a key role in the counter-flowing water masses (i.e. for $\Omega = 0.05\, rad/s$, Figure 5b), a tilt in the interface is observed and is coupled with the effect of the

increasing q^*, causing a significant deflection of the saline outflow on the right hand side of the trapezoidal channel.

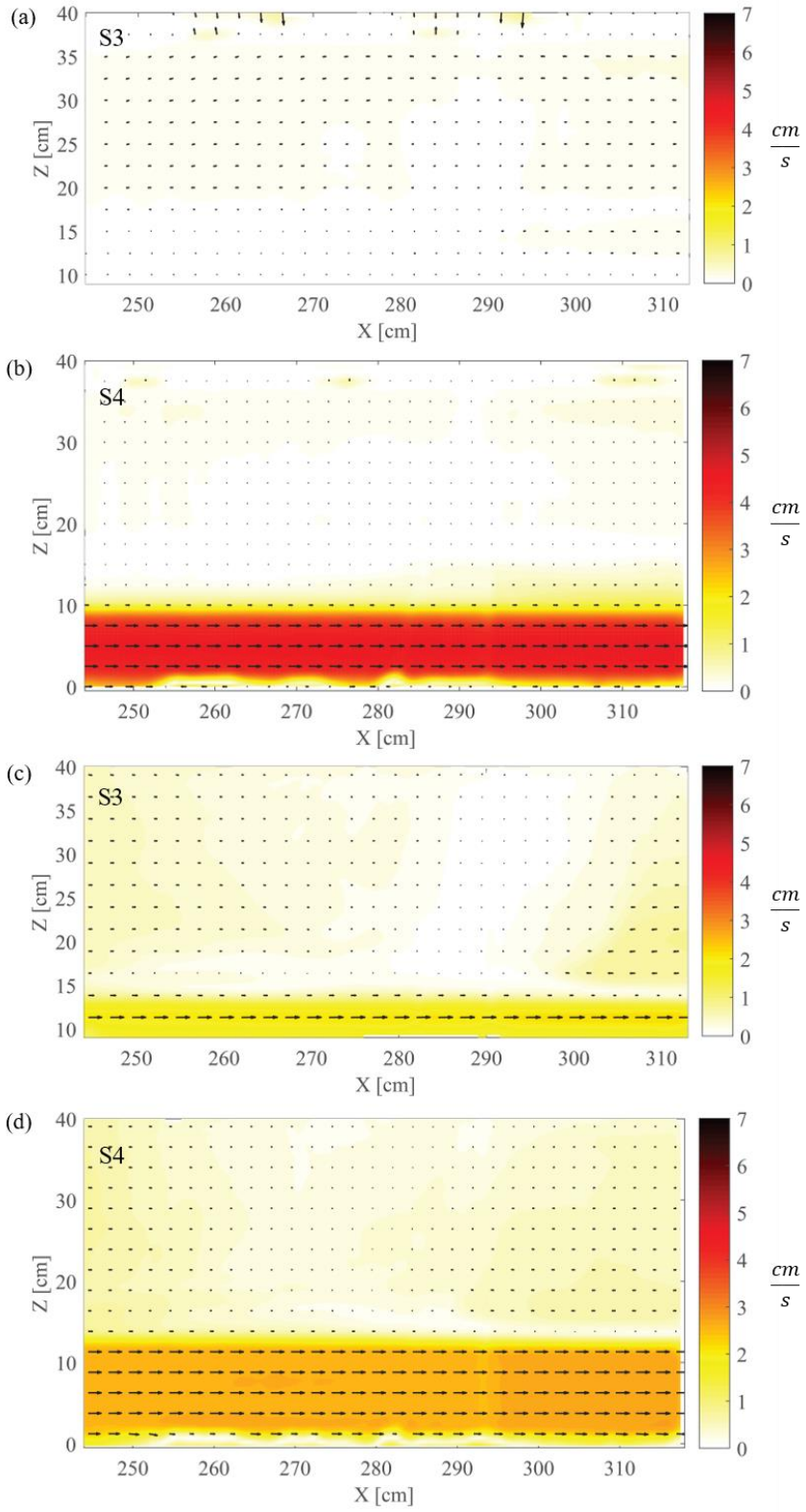

Figure 4 PIV velocity fields and colormap of the absolute value of u for gravity current experiments, i.e. q=0, for Ω=0 rad/s in PIV Section (a) S3 (i.e. y=-59.2 cm) and (b) S4 (i.e. y=-59.2 cm) and for Ω=0.05 rad/s in PIV Section (c) S3 and (d) S4.*

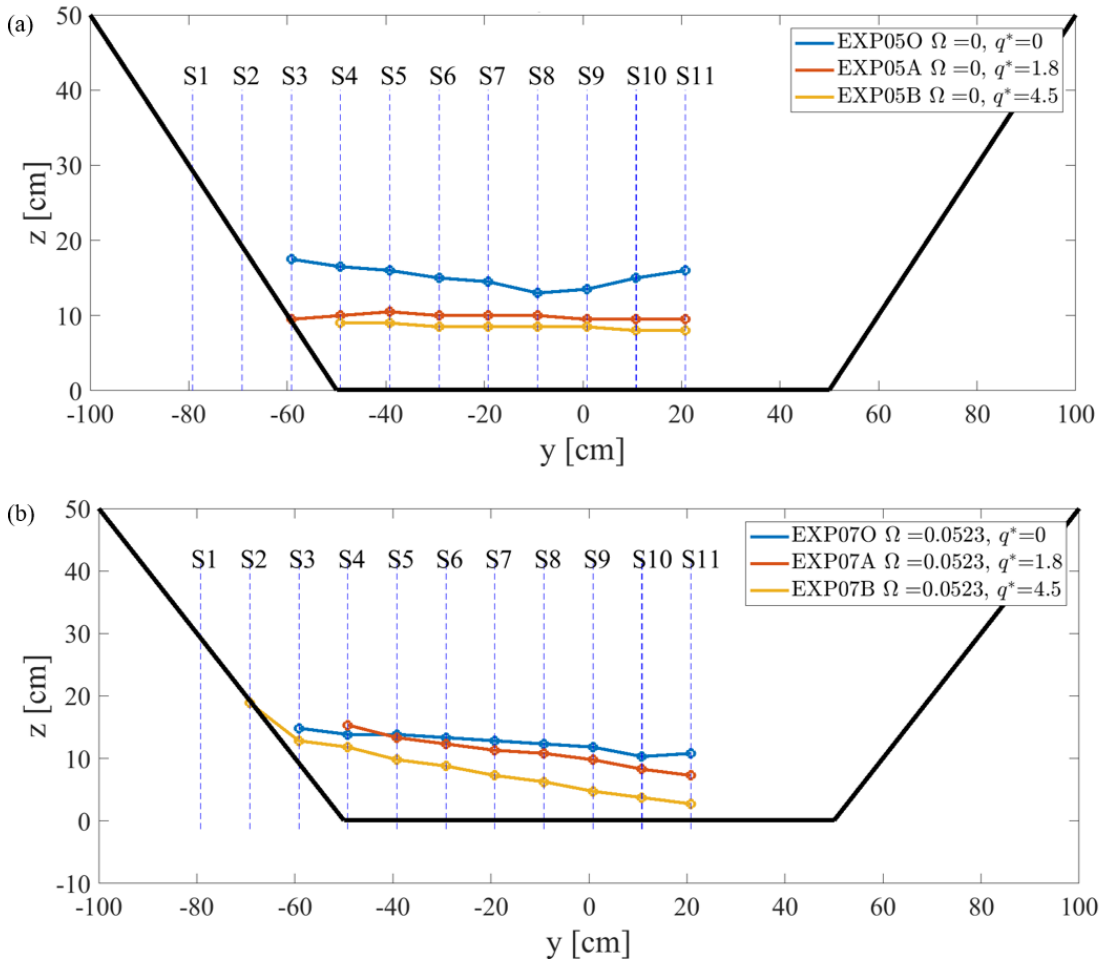

Figure 5 Cross channel $u = 0\ cm/s$ velocity interface in all the measured PIV sections, for increasing q and angular velocity (a) $\Omega = 0\ rad/s$ and (b) $\Omega = 0.05\ rad/s$*

CONCLUSIONS AND FUTURE DEVELOPMENTS

The present work deals with the initial analysis and preliminary findings from an experimental study conducted in the Coriolis Rotating Platform at LEGI Grenoble. Data analysis is ongoing to investigate how the channel cross-sectional shape influences the flow distribution, interfacial mixing and entrainment, secondary flow circulations, and near-bed dynamics in both uni and bi-directional, stratified, exchange flows, as well as to study the reciprocal feedback mechanisms generated between these exchange flow and the evolution of channel topography with an erodible bottom boundary. Access granted to the LEGI Coriolis Platform through the Hydralab+ Initiative has allowed a unique opportunity to conduct large-scale experiments on stratified, non-rotating and rotating exchange flows on both rigid-bottom and erodible bottom channels, within a wide parametric range of relevant geophysical conditions.

ACKNOWLEDGEMENT

"This project has received funding from the European Union's Horizon 2020 research and innovation programme under grant agreement No 654110, HYDRALAB+.".

REFERENCES

Andrejev, Myrberg, Alenius & Lundberg (2004). Mean circulation and water exchange in the Gulf of Finland – a study based on the three-dimensional modelling. Boreal Env. Res., 9, 1-16.

Cossu, Wells & Wåhlin (2010). Influence of the Coriolis force on the velocity structure of gravity currents in straight submarine channel systems, J. Geophy. Res., 115, C11016.

Cuthbertson A J S, Laanearu J & Davies P A (2006). Buoyancy-driven two-layer exchange flows across a slowly submerging barrier. Environ. Fluid Mech., 6, 133-151.

Cuthbertson A J S, Laanearu J, Wåhlin A K & Davies P A (2011). Experimental and analytical investigation of dense gravity currents in a rotating, up-sloping and converging channel. Dyn. Atmos. Oceans, 52(3), 386-409.

Cuthbertson A J S, Lundberg P, Davies P A & Laanearu J (2014). Gravity Currents in Rotating, Wedge-Shaped Adverse Channels. Environ. Fluid Mech., 14, 1251-1273.

Farmer & Armi (1999). Stratified flow over topography: the role of small-scale entrainment and mixing in flow establishment. Proc. Roy. Soc. A, 455, 3221-3258.

Johnson & Ohlson (1994). Frictionally modified rotating hydraulic channel exchange and ocean outflows. J. Phys. Ocean., 24(1), 66-78.

Kõuts & Omstedt (1993). Deep-water exchange in the Baltic Proper. Tellus A, 45, 311-324.

Laanearu J, Cuthbertson A J S & Davies P A (2014). Dynamics of dense gravity currents and mixing in an up-sloping and converging vee-shaped channel. J. Hyd. Res., 52(1), 67-80.

Matthäus & Lass (1995). The recent salt inflow into the Baltic Sea. J. Phys. Ocean., 25(2), 280-286.

Maxworthy (1985). On turbulent mixing across a density interface in the presence of rotation. J. Phys. Ocean., 16, 1136-1137.

Schramkowski & de Swart (2002). Morphodynamic equilibrium in straight tidal channels: Combined effects of Coriolis force and external overtides, J. Geophy. Res., 107(C12), 3227.

Valle-Levinson, Reyes & Sanay (2003). Effects of Bathymetry, Friction, and Rotation on Estuary–Ocean Exchange. J. Phys. Ocean., 33, 2375-2393.